AGU ADVANCING EARTH AND SPACE SCIENCE

Geophysical Research Letters

RESEARCH LETTER
10.1029/2021GL094078

Special Section:
Atmospheric Rivers: Intersection of Weather and Climate

Influence of Low-Frequency PNA Variability on MJO Teleconnections to North American Atmospheric River Activity

Kinya Toride[1,2] **and Gregory J. Hakim**[1]

[1]Department of Atmospheric Sciences, University of Washington, Seattle, WA, USA, [2]Institute of Industrial Science, The University of Tokyo, Kashiwa, Japan

Abstract The Madden-Julian oscillation (MJO) modulates atmospheric river (AR) activity along the West Coast of North America. The forecast skill of ARs based solely on the MJO phase is limited, motivating the identification of other predictive factors. Here we show that low-frequency variability of the Pacific/North American (PNA) pattern is mostly independent of the MJO, and the monthly PNA pattern influences the MJO-AR relationship much more robustly than other large-scale patterns such as the El Niño Southern Oscillation and the quasi-biennial oscillation. During PNA+ conditions, when the Pacific jet exit region is located further east than average, baroclinic wave packets extend downstream toward North America. The clear contrast in wave packets' zonal scale results in partitioning active and inactive AR phases. The PNA influence is most significant over the Pacific Northwest region of North America, where AR landfall is most frequent, with implied forecasting skill beyond 20 days.

Plain Language Summary The West Coast of North America often experiences heavy rainfall due to narrow bands of intense water vapor transport, called atmospheric rivers (ARs). Previous research showed slow oscillations in the tropical atmosphere modulate AR activity, indicating the potential of AR forecasts in the sub-seasonal time scale (3–5 weeks). However, the relationship is influenced by the structure and the configuration of the extratropical state. Here we show that monthly values of the Pacific/North American index of the extratropical Pacific atmosphere clearly classifies the essential relationship. The results suggest that the strength of the Aleutian low and the Pacific jet stream are the key drivers of the relationship, by guiding storms toward the West Coast of North America. We demonstrate that AR activity over the Pacific Northwest region in particular may be skillfully forecast for more than 20 days.

Key Points:

- Low-frequency variations in the Pacific/North American (PNA) pattern play a major role in modulating Madden-Julian oscillation (MJO) teleconnections to atmospheric river (AR) activity over the Northeast Pacific
- Aleutian low intensity and Pacific jet extension/retraction roughly partition active and inactive AR phases
- AR composites suggest forecasting skill potentially up to 3 weeks by using both MJO and monthly PNA phases

Supporting Information:

Supporting Information may be found in the online version of this article.

Correspondence to:

K. Toride,
kinyat@uw.edu

Citation:

Toride, K., & Hakim, G. J. (2021). Influence of low-frequency PNA variability on MJO teleconnections to North American atmospheric river activity. *Geophysical Research Letters*, *48*, e2021GL094078. https://doi.org/10.1029/2021GL094078

Received 26 APR 2021
Accepted 7 JUN 2021

1. Introduction

Atmospheric rivers (ARs), long and narrow regions of enhanced water vapor transport in the lower troposphere, are responsible for a significant fraction of extratropical moisture transport (Newman et al., 2012; Ralph et al., 2004; Zhu & Newell, 1998) and are associated with hydrological extremes in the mid-latitude continental region (Dettinger et al., 2011; Toride et al., 2019; Warner et al., 2012). There is intense interest in skillful AR forecasts in the sub-seasonal time scale (3–5 weeks) to prepare for high-impact hydrological events. Although previous studies investigated influences of many modes of climate variability on ARs, the Madden-Julian-Oscillation (MJO) is likely a primary driver of AR activity along the West Coast of North America on sub-seasonal timescales (Baggett et al., 2017; Guan et al., 2012; Mundhenk et al., 2018; Mundhenk, Barnes, & Maloney, 2016; Payne & Magnusdottir, 2016; Ralph et al., 2011). The MJO is an eastward-moving tropical disturbance that excites extratropical planetary wave propagation and modifies the midlatitude waveguide (e.g., Hoskins & Karoly, 1981; Matthews et al., 2004; Sardeshmukh & Hoskins, 1988). As a result, we expect AR frequency is modulated by the downstream development of wave packets (troughs and ridges) along the North Pacific storm track.

Uncertainty remains on the predictive skill of AR forecasts for North America based solely on the MJO phase, and how to supplement the MJO phase with other information. The propagation of planetary waves is sensitive to changes in the extratropical mean state and changes in the MJO heating structure (e.g., Hoskins & Ambrizzi, 1993). For this reason, previous studies have investigated including the quasi-biennial oscillation (QBO) phase on AR forecasts based on MJO (Baggett et al., 2017; Mundhenk et al., 2018). The

mechanisms of QBO impacts are through its influences on MJO propagation speed and intensity (Yoo & Son, 2016) and the teleconnection to the extratropical troposphere in winter (Andrews et al., 2019; Baldwin et al., 2001). Similarly, the El Niño Southern Oscillation (ENSO) can influence the MJO teleconnection by modifying the convective activity of MJO and Pacific jet stream structure (Lee et al., 2019; Moon et al., 2011; Tseng et al., 2020). Thus, North American AR forecasts are affected by MJO teleconnections through complex influences on both the Pacific jet basic state and the MJO forcing.

Here we test the hypothesis that the Pacific/North American (PNA) pattern, one of the representative indices of the extratropical state of the North Pacific (Wallace & Gutzler, 1981), is a useful predictor for the MJO-AR relationship using a reanalysis data set and a long climate model simulation. The hypothesis is supported by modeling studies that showed changes to the Pacific jet mean state have more substantial impacts on the MJO teleconnection than changes in MJO heating (Henderson et al., 2017; Zhou et al., 2020). Although the PNA on a daily timescale is affected by the MJO (Mori & Watanabe, 2008; Seo & Lee, 2017; Tseng et al., 2019), here we focus on the low-frequency component of PNA as captured by monthly averages. On these timescales, the PNA is associated with variability of the time-averaged Aleutian low and Pacific jet, with established connections to storm tracks and baroclinic wave propagation (e.g., Athanasiadis et al., 2010; Trenberth & Hurrell, 1994). In fact, it has been shown that combining MJO and PNA information is effective for U.S. temperature forecasts (Schreck et al., 2013). We demonstrate that the monthly PNA index increases the number of days with the significant MJO-AR lag relationship by more than a factor of two when compared to ENSO and QBO indices in the Pacific Northwest region.

2. Methods

2.1. Datasets

Atmospheric fields are taken from the Modern-Era Retrospective analysis for Research and Applications, Version 2 (MERRA-2; Gelaro et al., 2017) on isobaric surfaces. We use daily fields interpolated to a horizontal resolution of 2.5° by 2.5° in boreal winter (November to March; NDJFM) during 1980–2019. Precalculated integrated vapor transport (IVT) fields are obtained from the Atmospheric River Tracking Method Intercomparison Project (ARTMIP; Shields et al., 2018), which uses the horizontal wind components and specific humidity from 1,000 hPa to 200 hPa. We also obtain gridded AR tracks by Pan & Lu (2019) from the ARTMIP repository. Daily anomaly fields are calculated by subtracting the first four harmonics of the annual cycle based on the 1980–2019 period at every grid point. A 3–8 day Lanczos bandpass filter is applied to meridional wind anomalies to analyze synoptic-scale baroclinic waves. In addition to the MERRA2 data set, we also test the hypothesis on a 165-year climate model simulation, which is described in Section 4.

The Real-Time Multivariate MJO (RMM) index (Wheeler & Hendon, 2004) is used to categorize the MJO life cycle into eight phases, and to organize MJO phase composites. We use only active MJO phases (RMM amplitude greater than one) in this study (see Figure S1 for sample sizes). ENSO conditions are characterized by the oceanic Niño index (ONI), which is defined by a 3-month running mean of sea surface temperature anomalies in the Niño 3.4 region (170°W–120°W, 5°S–5°N). Monthly and daily PNA index values, and monthly QBO index values, are obtained from the National Oceanic and Atmospheric Administration/Climate Prediction Center (NOAA/CPC). The PNA index is calculated by projecting the 500 hPa geopotential height anomaly field onto its empirical orthogonal function loading pattern (Barnston & Livezey, 1987). The QBO index is a standardized monthly 50-hPa zonal wind anomaly in the equator region (e.g., Baldwin et al., 2001).

Negative/positive phases of ENSO, PNA, and QBO are defined as below/above 0.5 standard deviations of zero based on respective monthly indices. While the daily PNA index has high phase coherence with the MJO (Mori & Watanabe, 2008), there are nearly equal samples of monthly PNA+ and PNA− days for each RMM phase, which implies that MJO and PNA have no clear relationship on monthly time scales (Figure S1). In this work, we focus on monthly PNA unless otherwise specified. Although ENSO exhibits a qualitatively similar extratropical teleconnection pattern to PNA (Figure S2), the correlation between monthly ONI and PNA indices is only 0.14 for all months and 0.29 for NDJFM (Figure S3), indicating ENSO is only weakly related to monthly PNA variability; most monthly PNA variability is driven by other sources.

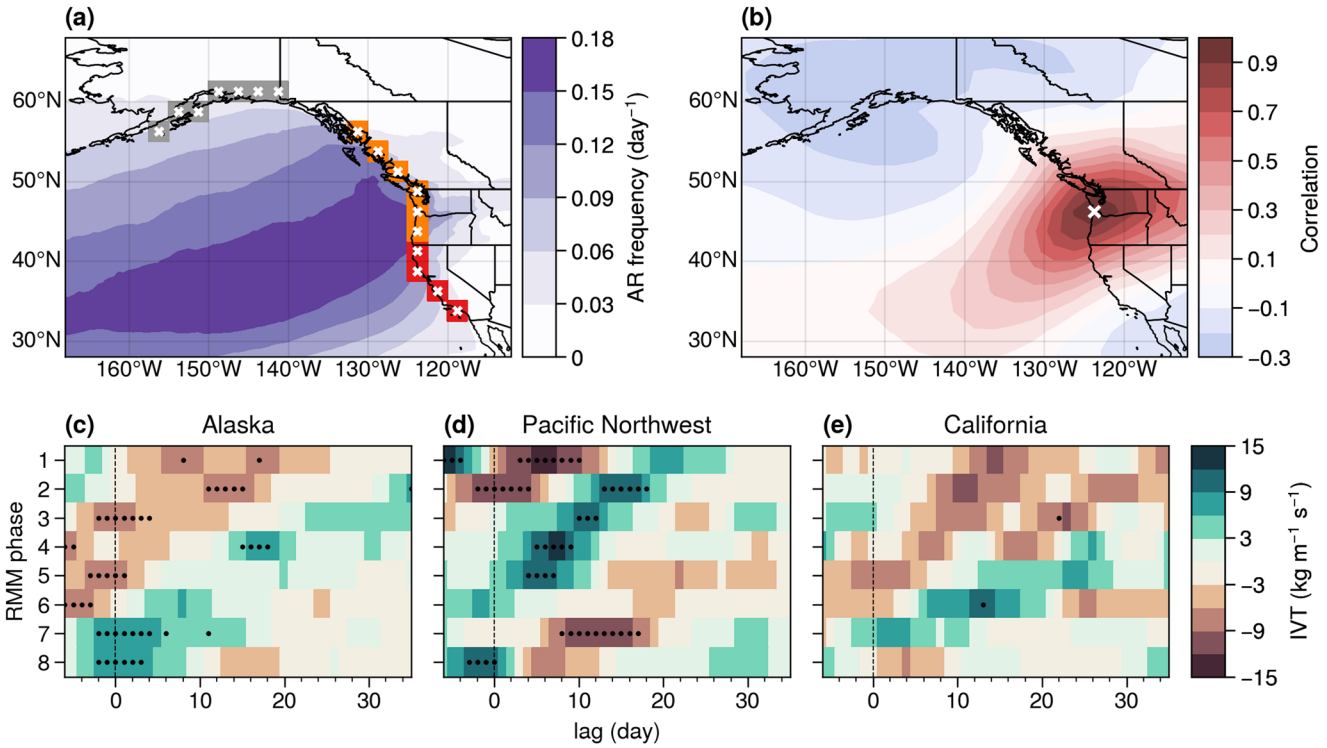

Figure 1. Study area and Madden-Julian oscillation (MJO) modulation of atmospheric river (AR) activity. (a) Location of Alaska (gray), Pacific Northwest (orange), and California (red) regions overlaying the AR mean frequency (shading; day^{-1}) based on Pan & Lu (2019) in November to March (NDJFM). (b) One-point correlation map of NDJFM integrated vapor transport (IVT). The white "x" mark shows the base point. Lag composites of anomalous IVT (kg m^{-1} s^{-1}) as a function of the MJO phase for (c) Alaska, (d) Pacific Northwest, and (e) California. Stippling denotes statistical significance at the 5% level.

Lag composites based on the MJO phase are constructed by conditioning on monthly averaged values for these climate modes to study their relationship. To test the statistical significance of composite anomalies, we perform a Monte Carlo test with 1,000 realizations by randomly shifting the original time series by sampling a discrete uniform distribution on the interval of 1 to N, where N is the total number of boreal winter dates (Seo & Lee, 2017; Zheng et al., 2018). We employ a circular resampling, where the end of the original time series is appended to the beginning to avoid undersampling near the edges of the original time series (Wilks, 2019). A null hypothesis is then constructed by producing composites from the shifted time series using the original MJO starting dates. Since each RMM phase typically lasts for multiple days (i.e., persistence in time), this method maintains the autocorrelation structure of the MJO time series. A composite anomaly is considered statistically significant based on the 95% confidence interval estimated from the null hypothesis.

2.2. Atmospheric River Activity

In this study, AR activity is diagnosed using anomalous IVT over the Pacific coastal regions of North America. IVT anomalies are averaged over the Alaska, Pacific Northwest, and California regions as shown in Figure 1a. Then, a 5-day running mean is applied to the anomalous IVT time series for each region. AR landfall is most frequent in the Pacific Northwest region, followed by California. Figure 1b reveals the spatial scale of ARs, where AR activity in the Pacific Northwest and the Gulf of Alaska are anticorrelated due to the northeastern Pacific height structure. We also diagnose AR activity based on tracking AR events by various methods available in ARTMIP, and overall results are similar (not shown). By using IVT, we can analyze the magnitude of AR signals in units of vapor flux.

Figures 1c–1e show the lag composites of AR activity over the three regions based solely on the MJO phase (referred to as MJO-AR relationship). In all regions, periodic IVT fluctuations are evident in response to the MJO life cycle, consistent with the results of Mundhenk et al. (2018). The days following Phase 3, when the

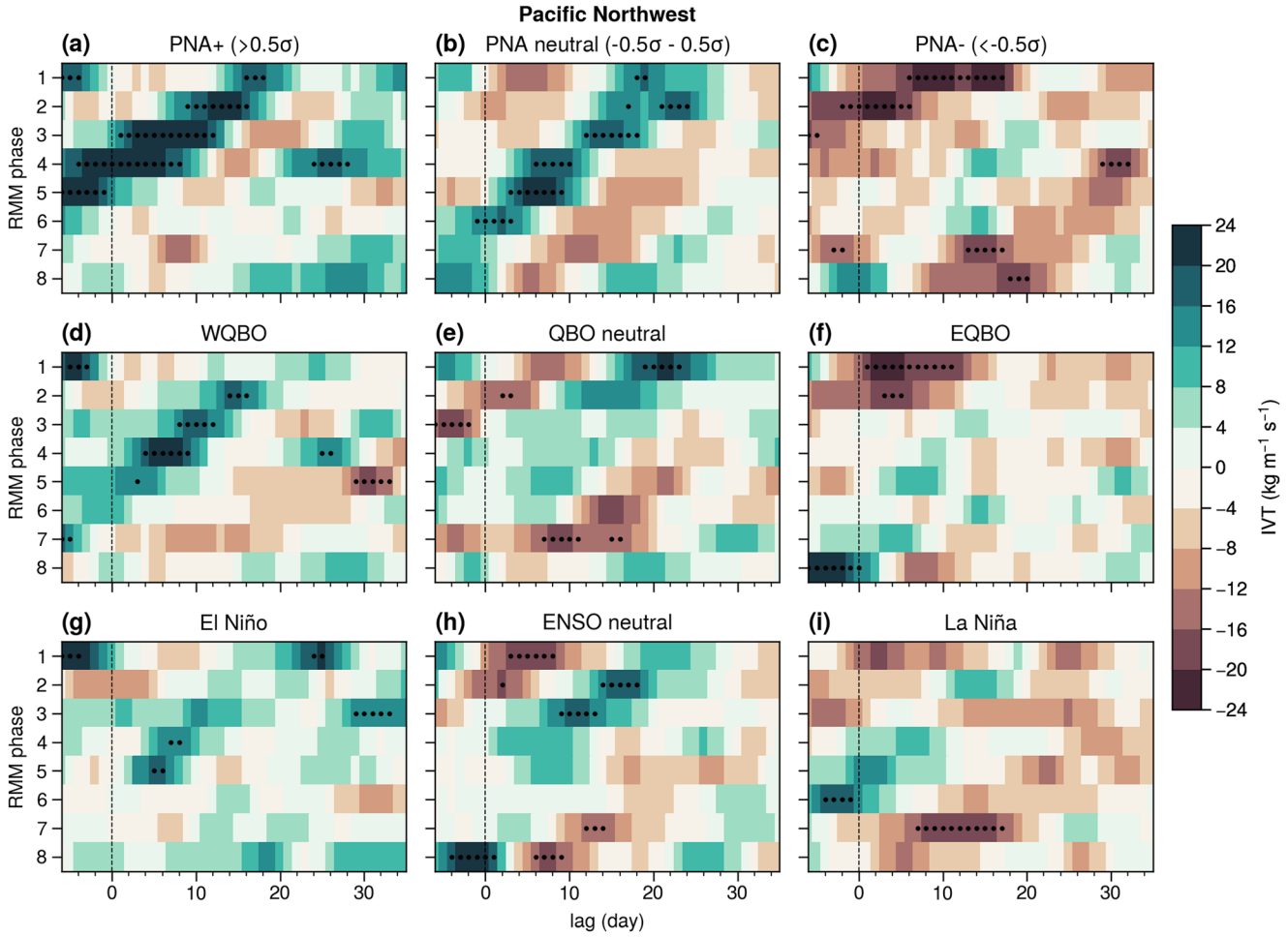

Figure 2. Lag composites of anomalous integrated vapor transport (kg m^{-1} s^{-1}) over Pacific Northwest as a function of Madden-Julian oscillation phase conditioned on monthly (a–c) Pacific/North American, (d–f) quasi-biennial oscillation, and (g–i) El Niño Southern Oscillation phases. Stippling denotes statistical significance at the 5% level.

heating is active over the Indian Ocean, are characterized by increased AR activity over the Pacific Northwest and decreased AR activity over Alaska and California. The MJO-AR relationships in these regions for this MJO phase are in line with the negative correlations in Figure 1b, revealing the spatial scale of AR activity. According to the Monte Carlo tests, these signals are most significant in the Pacific Northwest, less significant in Alaska, and not significant in California (Figures 1c–1e). As a result, for the rest of the study, we focus on results for the Pacific Northwest region; results for Alaska and California are shown in the Supplement.

3. Results

Figure 2 summarizes the MJO-AR relationship conditioned on positive, neutral, and negative phases of the monthly PNA, QBO, and ONI indices in the Pacific Northwest. Figures 2a–2c reveal that AR activity is clearly related to the monthly PNA phase, with an increase (decrease) in AR activity during PNA+ (PNA−). There is also increased AR activity for neutral PNA conditions, with a shift toward a larger RMM phase at a shorter lag time compared to the PNA+ case (Figure 2b). Positive anomalous IVT is enhanced, and negative anomalous IVT is weakened in the PNA neutral case when compared to the unconditioned results in Figure 1d. A second AR event signal is also evident during PNA+ at about lag 25 days following RMM Phase 4. Decreased IVT is statistically significant at lags up to ~30 days following Phase 4 in the PNA− condition.

Increased AR activity can also be detected during the westerly phase of the QBO (WQBO; Figure 2d) as shown by previous studies (Baggett et al., 2017; Mundhenk et al., 2018). IVT anomalies during QBO neutral conditions (Figure 2e) are similar to the unconditioned case (Figure 1d), but statistically significant signals are reduced. IVT changes are only significant after MJO phases 1 and 2 during EQBO (Figure 2f). Overall, the increased and decreased signals associated with the QBO phase are not as consistent, and not as robust, as those for the PNA. Figures 2g–2i show that ENSO conditioning exhibits similar, but reduced, IVT signals as those compared to the PNA (Figures 2a–2c), possibly because PNA partly manifests ENSO's modulation of the mid-latitude Pacific region. Increased and decreased IVT signals appear during El Niño and La Niña, respectively, but signal amplitude is smaller and shifted relative to the PNA case. ENSO neutral conditions exhibit similar signals to the unconditioned case and PNA+, but with smaller amplitude. In total, the number of days with statistically significant signals is 95 days when the MJO-AR relationship is conditioned by the PNA index during lags of 0–30 days, which is more than twice those for QBO (46 days) and ENSO (42 days). The PNA index classifies the MJO-AR relationship similarly in California and Alaska (Text S1).

Next, we compare the magnitude and pattern of the extratropical anomalous structure for the monthly indices conditioned on RMM Phase 3. Recall that during PNA+, AR activity significantly increases at lag 1–12 days following RMM Phase 3 over the Pacific Northwest. Figure 3 shows the 500 hPa geopotential height anomaly and 250 hPa zonal wind composites over the North Pacific for each climate mode for RMM Phase 3. The MJO-AR relationship can be roughly classified into the PNA+, WQBO, El Niño group (active AR in the Pacific Northwest), and the PNA−, EQBO, La Niña group (inactive AR in the Pacific Northwest) based on Figures 2, S4 and S5. This classification can be explained by the strength and sign of the 500 hPa height anomaly over the central North Pacific. RMM Phase 3 (convection over the Indian Ocean) is typically associated with a positive height anomaly over the central North Pacific (Zheng & Chang, 2019). The positive height anomaly weakens during PNA+, WQBO, and El Niño, and strengthens during PNA−, EQBO, and La Niña, indicating that the strength of the Aleutian low is a primary influence on the MJO-AR relationship for the Pacific Northwest. The magnitude of height changes associated with the PNA is about three times as large as those for QBO and ENSO. Moreover, the Pacific jet-exit region is zonally shifted eastward by more than 20° longitude for PNA+ compared to PNA−. The extension/retraction of the Pacific jet in association with the PNA is accompanied by spatial shifts in the storm track (e.g., Athanasiadis et al., 2010), and affects trough-ridge development over the Northeast Pacific (Jaffe et al., 2011), which explains the clear division of AR signals seen in Figures 2a–2c. The height anomaly induced by ENSO has a similar but weaker pattern, shifted to the east, when compared to the PNA result (Figures 3e and 3f), which is consistent with the AR activity results. The QBO teleconnection exhibits weaker patterns, and the Pacific jet is close to the climatological position (Figures 3c and 3d).

These results reveal that changes in the Pacific jet influence the MJO-AR teleconnection pattern. In order to connect these changes to the primary features that produce AR events, baroclinic waves, we now consider how the structural changes to the jet affect the statistics of baroclinic waves. Specifically, we anticipate that baroclinic wave packets propagating along the mid-latitude waveguide are affected by the position of the jet exit region over the central Pacific. As shown by previous studies (e.g., Chang, 1993; Wallace et al., 1988), one-point correlation maps of upper-level meridional wind are useful to diagnose baroclinic wave trains. Figure 3 shows one-point correlation maps of 3–8 day bandpass-filtered meridional wind with a base point at (36.25°N, 171.25°W) near the jet exit region. During PNA+ conditions, when the jet exit is located further east than average, baroclinic wave packets are zonally stretched and extend from east Asia to North America. In contrast, the zonal scale of wave packets is much smaller during PNA−, with equatorward refraction of the waves prior to reaching the West Coast of North America. Similar to the jet extension/retraction result, changes in the zonal scales of wave packets are most robust for PNA compared to QBO and ENSO: the zonal retraction is particularly strong during PNA−. The Hovmöller diagrams in Figure S6 also indicate that the low-frequency wave train from the eastern Pacific following MJO Phase 3 (Cassou, 2008) is most pronounced during PNA+, and damped during PNA−. The orientation and horizontal scale of baroclinic waves can also affect ARs through wave-breaking structure, which influences the meridional distribution of AR landfalls (Hu et al., 2017; Mundhenk, Barnes, Maloney & Nardi, 2016).

These contrasts in the zonal scale of the Pacific jet associated with the PNA pattern can be seen in other RMM phases as well (Figure S7a). Although the jet's zonal scale changes with the MJO phase, it is

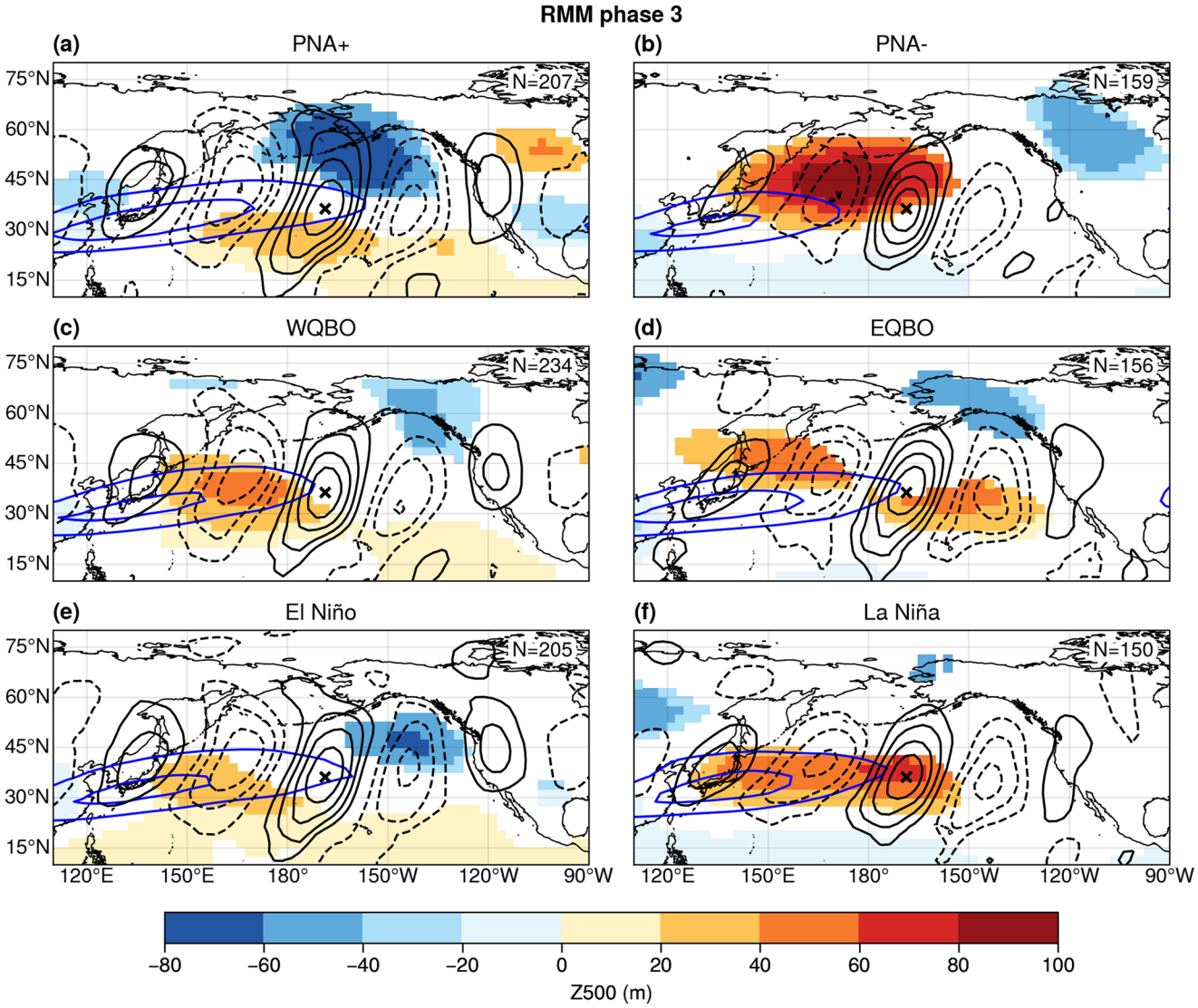

Figure 3. Geopotential height anomaly at 500 hPa (shading; m) and zonal wind at 250 hPa (blue contours at 40 and 55 m s^{-1}) composited for Real-Time Multivariate Madden-Julian oscillation Phase 3 and monthly (a) PNA+, (b) PNA−, (c) WQBO, (d) EQBO, (e) El Niño, and (f) La Niña in November to March. Geopotential height anomalies are shown only where statistical significance is at the 5% level. Black contours show one-point correlation maps of 3–8 day bandpass-filtered meridional wind anomaly at 250 hPa (0.2 intervals, 0 is not shown). The black "x" denotes the base point (36.25°N, 171.25°W). The numbers of days are shown in the upper right corner.

consistently longer during PNA+ compared to during PNA−. Interestingly, the effects of PNA appear to be basically a linear superposition on the MJO teleconnection patterns. Figure S7 demonstrates that when composites based on MJO alone and composites based on PNA alone are superimposed, they generally show similar height patterns to the composites conditioned on both MJO and PNA. While the PNA pattern is often associated with the MJO on a daily timescale (Mori & Watanabe, 2008; Seo & Lee, 2017; Tseng et al., 2019), our results suggest that the PNA has low-frequency variability independent of MJO that strongly affects AR activity along the West Coast of North America.

The above results are based on monthly indices, which cannot be effectively used for daily forecasting. Figure 4 shows lag IVT composites conditioned on the daily PNA index (Figures 4a–4c) and the daily PNA index with a running-mean average over the 30 days before the MJO phase (Figures 4d–4f) for the Pacific Northwest. When conditioned on the unsmoothed daily PNA index, the lag composites emphasize AR activity at lag 0 almost regardless of the MJO phase, showing the close relationship between AR and the

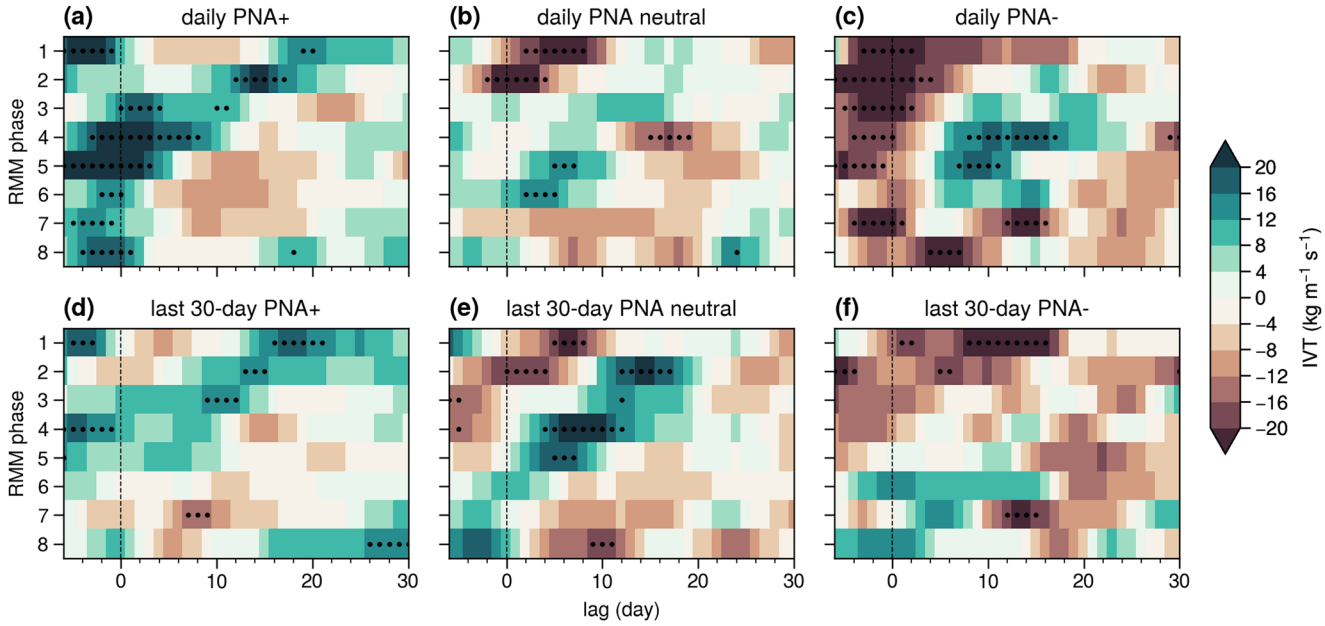

Figure 4. Lag composites of anomalous integrated vapor transport (kg m^{-1} s^{-1}) over the Pacific Northwest as a function of Madden-Julian oscillation phase conditioned on (a–c) daily Pacific/North American (PNA), and (d–f) previous 30-day-average PNA index. Stippling denotes statistical significance at the 5% level.

Aleutian low (Guan & Waliser, 2015). In contrast, although the signals become somewhat weaker than those in Figures 2, 4d and 4f show a clear symmetry in AR activity conditioned upon the previous 30-day-average PNA index. Increased (decreased) AR activity is consistent in days following RMM phases during PNA+ and PNA neutral (PNA−). These results suggest the potential of enhanced AR predictive skill based on the MJO phase and the previous 30-day-average PNA index.

4. GFDL-CM4 CMIP6 Simulation

In this study, the relationship of the MJO to AR activity is analyzed based on the 40-year period covered by MERRA-2. Although each active MJO phase has a sample size of ~500, the number of independent MJO samples is much smaller (~100) because each phase lasts for 5 consecutive days on average. Thus, to increase the sample size (to about ~400 independent samples), we conduct a similar analysis using the 165-year climate model simulation from GFDL-CM4 as contributed to the Couple Modeled Intercomparison Project Phase 6 (CMIP6; Eyring et al., 2016). The GFDL-CM4 simulates good MJO propagation based on the precipitation east-west power ratio (https://pcmdi.llnl.gov/pmp-preliminary-results/mjo_metrics/mjo_ewr_cmip5and6_overlap_runs_average_standalone.html) and the Maritime Continent propagation metric (Ahn et al., 2020). Text S2 provides the details regarding CMIP6 data and data processing.

The modeled MJO teleconnection to AR activity is overall similar to the results from the reanalysis (Figure S8). The signals are consistent among RMM phases both for the Pacific Northwest and Alaska. A phase reversal between the Pacific Northwest and Alaska is also evident, similar to that in the MERRA-2 results. The propagation of the AR signal is damped over California compared to the reanalysis results, possibly due to the differences in the meridional distribution of IVT (Warner et al., 2015). When subdivided by climate modes as for the MERRA-2 analysis, the monthly PNA index separates the anomalous AR activity most clearly in the Pacific Northwest (Figure S9), in line with the reanalysis results. Increased and decreased AR signals are statistically significant for more than 20 days and have larger magnitudes than those conditioned on the other indices considered here. The PNA and ONI indices provide more robust AR activity signals than the QBO in Alaska (Figure S10), whereas the most significant signals are obtained for ENSO conditions in California (Figure S11). The number of days with statistically significant signals is largest when conditioned on the PNA in the Pacific Northwest and Alaska during lag days 0–30. In summary, this

CMIP6-model-based analysis provides a much larger sample that yields results mostly consistent with the reanalysis results.

5. Conclusions

The present study shows that the monthly PNA index is useful for predicting the MJO influence on AR activity along the West Coast of North America based on a diagnostic analysis using a reanalysis data set and climate model data. The AR signals are most significant and robust when conditioned on monthly PNA values as compared to ENSO or QBO along the West Coast of North America. Because the monthly mean PNA index accounts for the variability of Aleutian low intensity and Pacific jet stream extension/retraction, the results highlight the importance of the extratropical jet on linking MJO structure to AR activity. To leading order, Aleutian low strength is key to the AR activity because it modulates baroclinic wave propagation across the North Pacific. Indeed, AR activity can be roughly classified into two groups (i.e., PNA+, WQBO, El Niño group; and PNA−, EQBO, La Niña group) according to the strength and sign of geopotential height anomaly over the central North Pacific. When the jet exit region extends eastward during PNA+, baroclinic waves are zonally stretched and directed more poleward into North America following the RMM Phase 3, which could modify the meridional distribution of AR landfall. The effects of low-frequency PNA variability appear to be mostly independent of the MJO, and we find that a linear superimposition of MJO and PNA teleconnection patterns recovers the main results for composites conditionally sampled on both the MJO and monthly mean PNA. The contrast of the Pacific jet's zonal scale during PNA+ and PNA− phases is the main reason for the clear division in the MJO-AR relationship.

The results of this study suggest a need for a better understanding of baroclinic wave evolution on different Pacific-jet basic states in relation to AR activity. In particular, differences in the phasing of baroclinic wave packets appear to be important relative to the large-scale structure of the Pacific jet (i.e., the PNA phase). Furthermore, although the daily evolution of PNA has been extensively studied (Henderson et al., 2020; Mori & Watanabe, 2008; Seo & Lee, 2017; Tseng et al., 2019), the relationship between low-frequency PNA variability and MJO activity is less well understood and the subject of future study. The relative importance of two factors (forcing from MJO heating and Pacific-jet basic state structure) also needs to be clarified to explain the physical mechanisms of ENSO and QBO influences on AR activity along the West Coast of North America.

Data Availability Statement

All data used in this paper can be downloaded from the following: MERRA-2 https://disc.gsfc.nasa.gov/; ARTMIP data, https://doi.org/10.5065/D62R3QFS and https://doi.org/10.5065/D6R78D1M; CMIP6 data, https://esgf-node.llnl.gov/search/cmip6/; RMM index, http://www.bom.gov.au/climate/mjo/; PNA index, https://www.cpc.ncep.noaa.gov/products/precip/CWlink/pna/pna.shtml; QBO index, https://www.cpc.ncep.noaa.gov/data/indices/qbo.u50.index; ONI index, https://psl.noaa.gov/data/correlation/oni.data.

Acknowledgments
This work was supported by JSPS KAKENHI Grant 19J01337 and 20K14833. GJH was supported by NOAA grant NA20NWS4680053.

References

Ahn, M. M., Kim, D., Kang, D., Lee, J., Sperber, K. R., Gleckler, P. J., et al. (2020). MJO Propagation across the Maritime continent: Are CMIP6 models better than CMIP5 models? *Geophysical Research Letters*, *47*(11), e2020GL087250. https://doi.org/10.1029/2020GL087250

Andrews, M. B., Knight, J. R., Scaife, A. A., Lu, Y., Wu, T., Gray, L. J., & Schenzinger, V. (2019). Observed and simulated teleconnections between the stratospheric quasi-biennial oscillation and Northern Hemisphere winter atmospheric circulation. *Journal of Geophysical Research: Atmospheres*, *124*(3), 1219–1232. https://doi.org/10.1029/2018JD029368

Athanasiadis, P. J., Wallace, J. M., & Wettstein, J. J. (2010). Patterns of wintertime jet stream variability and their relation to the storm tracks. *Journal of the Atmospheric Sciences*, *67*(5), 1361–1381. https://doi.org/10.1175/2009JAS3270.1

Baggett, C. F., Barnes, E. A., Maloney, E. D., & Mundhenk, B. D. (2017). Advancing atmospheric river forecasts into subseasonal-to-seasonal time scales. *Geophysical Research Letters*, *44*(14), 7528–7536. https://doi.org/10.1002/2017GL074434

Baldwin, M. P., Gray, L. J., Dunkerton, T. J., Hamilton, K., Haynes, P. H., Randel, W. J., et al. (2001). The quasi-biennial oscillation. *Reviews of Geophysics*, *39*(2), 179–229. https://doi.org/10.1029/1999RG000073

Barnston, A. G., & Livezey, R. E. (1987). Classification, seasonality and persistence of low-frequency atmospheric circulation patterns. *Monthly Weather Review*, *115*(6), 1083–1126. https://doi.org/10.1175/1520-0493(1987)115<1083:CSAPOL>2.0.CO;2

Cassou, C. (2008). Intraseasonal interaction between the Madden–Julian Oscillation and the North Atlantic Oscillation. *Nature*, *455*(7212), 523–527. https://doi.org/10.1038/nature07286

Chang, E. K. M. (1993). Downstream development of baroclinic waves as inferred from regression analysis. *Journal of the Atmospheric Sciences*, *50*(13), 2038–2053. https://doi.org/10.1175/1520-0469(1993)050<2038:DDOBWA>2.0.CO;2

Dettinger, M. D., Ralph, F. M., Das, T., Neiman, P. J., & Cayan, D. R. (2011). Atmospheric rivers, floods and the water resources of California. *Water*, *3*(2), 445–478. https://doi.org/10.3390/w3020445

Eyring, V., Bony, S., Meehl, G. A., Senior, C. A., Stevens, B., Stouffer, R. J., & Taylor, K. E. (2016). Overview of the Coupled Model Intercomparison Project Phase 6 (CMIP6) experimental design and organization. *Geoscientific Model Development*, *9*(5), 1937–1958. https://doi.org/10.5194/gmd-9-1937-2016

Gelaro, R., McCarty, W., Suárez, M. J., Todling, R., Molod, A., Takacs, L., et al. (2017). The Modern-Era Retrospective Analysis for Research and Applications, Version 2 (MERRA-2). *Journal of Climate*, *30*(14), 5419–5454. https://doi.org/10.1175/JCLI-D-16-0758.1

Guan, B., & Waliser, D. E. (2015). Detection of atmospheric rivers: Evaluation and application of an algorithm for global studies. *Journal of Geophysical Research: Atmospheres*, *120*(24), 12514–12535. https://doi.org/10.1002/2015JD024257

Guan, B., Waliser, D. E., Molotch, N. P., Fetzer, E. J., & Neiman, P. J. (2012). Does the Madden–Julian oscillation influence wintertime atmospheric rivers and snowpack in the Sierra Nevada? *Monthly Weather Review*, *140*(2), 325–342. https://doi.org/10.1175/MWR-D-11-00087.1

Henderson, S. A., Maloney, E. D., & Son, S.-W. (2017). Madden–Julian oscillation pacific teleconnections: The impact of the basic state and MJO representation in general circulation models. *Journal of Climate*, *30*(12), 4567–4587. https://doi.org/10.1175/JCLI-D-16-0789.1

Henderson, S. A., Vimont, D. J., & Newman, M. (2020). The critical role of non-normality in partitioning tropical and extratropical contributions to PNA growth. *Journal of Climate*, *33*(14), 6273–6295. https://doi.org/10.1175/JCLI-D-19-0555.1

Hoskins, B. J., & Ambrizzi, T. (1993). Rossby wave propagation on a realistic longitudinally varying flow. *Journal of the Atmospheric Sciences*, *50*(12), 1661–1671. https://doi.org/10.1175/1520-0469(1993)050<1661:RWPOAR>2.0.CO;2

Hoskins, B. J., & Karoly, D. J. (1981). The steady linear response of a spherical atmosphere to thermal and orographic forcing. *Journal of the Atmospheric Sciences*, *38*(6), 1179–1196. https://doi.org/10.1175/1520-0469(1981)038<1179:TSLROA>2.0.CO;2

Hu, H., Dominguez, F., Wang, Z., Lavers, D. A., Zhang, G., & Ralph, F. M. (2017). Linking atmospheric river hydrological impacts on the U.S. West Coast to Rossby wave breaking. *Journal of Climate*, *30*(9), 3381–3399. https://doi.org/10.1175/JCLI-D-16-0386.1

Jaffe, S. C., Martin, J. E., Vimont, D. J., & Lorenz, D. J. (2011). A synoptic climatology of episodic, subseasonal retractions of the Pacific Jet. *Journal of Climate*, *24*(11), 2846–2860. https://doi.org/10.1175/2010JCLI3995.1

Lee, R. W., Woolnough, S. J., Charlton-Perez, A. J., & Vitart, F. (2019). ENSO modulation of MJO teleconnections to the North Atlantic and Europe. *Geophysical Research Letters*. https://doi.org/10.1029/2019GL084683

Matthews, A. J., Hoskins, B. J., & Masutani, M. (2004). The global response to tropical heating in the Madden–Julian oscillation during the northern winter. *Quarterly Journal of the Royal Meteorological Society*, *130*(601), 1991–2011. https://doi.org/10.1256/qj.02.123

Moon, J.-Y., Wang, B., & Ha, K.-J. (2011). ENSO regulation of MJO teleconnection. *Climate Dynamics*, *37*(5–6), 1133–1149. https://doi.org/10.1007/s00382-010-0902-3

Mori, M., & Watanabe, M. (2008). The growth and triggering mechanisms of the PNA: A MJO-PNA coherence. *Journal of the Meteorological Society of Japan*, *86*(1), 213–236. https://doi.org/10.2151/jmsj.86.213

Mundhenk, B. D., Barnes, E. A., & Maloney, E. D. (2016). All-season climatology and variability of atmospheric river frequencies over the North Pacific. *Journal of Climate*, *29*(13), 4885–4903. https://doi.org/10.1175/JCLI-D-15-0655.1

Mundhenk, B. D., Barnes, E. A., Maloney, E. D., & Baggett, C. F. (2018). Skillful empirical subseasonal prediction of landfalling atmospheric river activity using the Madden–Julian oscillation and quasi-biennial oscillation. *Npj Climate and Atmospheric Science*, *1*(1), 20177. https://doi.org/10.1038/s41612-017-0008-2

Mundhenk, B. D., Barnes, E. A., Maloney, E. D., & Nardi, K. M. (2016). Modulation of atmospheric rivers near Alaska and the U.S. West Coast by northeast Pacific height anomalies. *Journal of Geophysical Research: Atmospheres*, *121*(21), 12751–12765. https://doi.org/10.1002/2016JD025350

Newman, M., Kiladis, G. N., Weickmann, K. M., Ralph, F. M., & Sardeshmukh, P. D. (2012). Relative contributions of synoptic and low-frequency Eddies to time-mean atmospheric moisture transport, including the role of atmospheric rivers. *Journal of Climate*, *25*(21), 7341–7361. https://doi.org/10.1175/JCLI-D-11-00665.1

Pan, M., & Lu, M. (2019). A novel atmospheric river identification algorithm. *Water Resources Research*, *55*(7), 6069–6087. https://doi.org/10.1029/2018WR024407

Payne, A. E., & Magnusdottir, G. (2016). Persistent landfalling atmospheric rivers over the west coast of North America. *Journal of Geophysical Research: Atmospheres*, *121*(22), 13287–13300. https://doi.org/10.1002/2016JD025549

Ralph, F. M., Neiman, P. J., Kiladis, G. N., Weickmann, K., & Reynolds, D. W. (2011). A multiscale observational case study of a Pacific atmospheric river exhibiting tropical–extratropical connections and a mesoscale frontal wave. *Monthly Weather Review*, *139*(4), 1169–1189. https://doi.org/10.1175/2010MWR3596.1

Ralph, F. M., Neiman, P. J., & Wick, G. A. (2004). Satellite and CALJET aircraft observations of atmospheric rivers over the Eastern North Pacific Ocean during the winter of 1997/98. *Monthly Weather Review*, *132*(7), 1721–1745. https://doi.org/10.1175/1520-0493(2004)132<1721:SACAOO>2.0.CO;2

Sardeshmukh, P. D., & Hoskins, B. J. (1988). The generation of global rotational flow by steady idealized tropical divergence. *Journal of the Atmospheric Sciences*, *45*(7), 1228–1251. https://doi.org/10.1175/1520-0469(1988)045<1228:TGOGRF>2.0.CO;2

Schreck, C. J., Cordeira, J. M., & Margolin, D. (2013). Which MJO events affect north american temperatures? *Monthly Weather Review*, *141*(11), 3840–3850. https://doi.org/10.1175/MWR-D-13-00118.1

Seo, K.-H., & Lee, H.-J. (2017). Mechanisms for a PNA-like teleconnection pattern in response to the MJO. *Journal of the Atmospheric Sciences*, *74*(6), 1767–1781. https://doi.org/10.1175/JAS-D-16-0343.1

Shields, C. A., Rutz, J. J., Leung, L.-Y., Ralph, F. M., Wehner, M., Kawzenuk, B., et al. (2018). Atmospheric River Tracking Method Intercomparison Project (ARTMIP): Project goals and experimental design. *Geoscientific Model Development*, *11*(6), 2455–2474. https://doi.org/10.5194/gmd-11-2455-2018

Toride, K., Iseri, Y., Warner, M. D., Frans, C. D., Duren, A. M., England, J. F., & Kavvas, M. L. (2019). Model-based probable maximum precipitation estimation: How to estimate the worst-case scenario induced by atmospheric rivers? *Journal of Hydrometeorology*, *20*(12), 2383–2400. https://doi.org/10.1175/JHM-D-19-0039.1

Trenberth, K. E., & Hurrell, J. W. (1994). Decadal atmosphere-ocean variations in the Pacific. *Climate Dynamics*, *9*(6), 303–319. https://doi.org/10.1007/BF00204745

Tseng, K.-C., Maloney, E., & Barnes, E. (2019). The consistency of MJO teleconnection patterns: An explanation using Linear Rossby Wave Theory. *Journal of Climate*, *32*(2), 531–548. https://doi.org/10.1175/JCLI-D-18-0211.1

Tseng, K.-C., Maloney, E., & Barnes, E. A. (2020). The consistency of MJO teleconnection patterns on interannual time scales. *Journal of Climate*, *33*(9), 3471–3486. https://doi.org/10.1175/JCLI-D-19-0510.1

Wallace, J. M., & Gutzler, D. S. (1981). Teleconnections in the Geopotential Height Field during the Northern Hemisphere Winter. *Monthly Weather Review*, *109*(4), 784–812. https://doi.org/10.1175/1520-0493(1981)109<0784:TITGHF>2.0.CO;2

Wallace, J. M., Lim, G.-H., & Blackmon, M. L. (1988). Relationship between Cyclone Tracks, Anticyclone Tracks and Baroclinic Waveguides. *Journal of the Atmospheric Sciences*, *45*(3), 439–462. https://doi.org/10.1175/1520-0469(1988)045<0439:RBCTAT>2.0.CO;2

Warner, M. D., Mass, C. F., & Salathé, E. P. (2012). Wintertime extreme precipitation events along the Pacific Northwest Coast: Climatology and synoptic evolution. *Monthly Weather Review*, *140*(7), 2021–2043. https://doi.org/10.1175/MWR-D-11-00197.1

Warner, M. D., Mass, C. F., & Salathé, E. P. (2015). Changes in winter atmospheric rivers along the North American West Coast in CMIP5 Climate Models. *Journal of Hydrometeorology*, *16*(1), 118–128. https://doi.org/10.1175/JHM-D-14-0080.1

Wheeler, M. C., & Hendon, H. H. (2004). An all-season real-time multivariate MJO Index: Development of an index for monitoring and prediction. *Monthly Weather Review*, *132*(8), 1917–1932. https://doi.org/10.1175/1520-0493(2004)132<1917:AARMMI>2.0.CO;2

Wilks, D. S. (2019). *Statistical methods in the atmospheric sciences*. Elsevier. https://doi.org/10.1016/C2017-0-03921-6

Yoo, C., & Son, S. (2016). Modulation of the boreal wintertime Madden-Julian oscillation by the stratospheric quasi-biennial oscillation. *Geophysical Research Letters*, *43*(3), 1392–1398. https://doi.org/10.1002/2016GL067762

Zheng, C., & Chang, E. K. M. (2019). The role of MJO propagation, lifetime, and intensity on modulating the temporal evolution of the MJO extratropical response. *Journal of Geophysical Research: Atmospheres*, *124*(10), 5352–5378. https://doi.org/10.1029/2019JD030258

Zheng, C., Kar-Man Chang, E., Kim, H.-M., Zhang, M., & Wang, W. (2018). Impacts of the Madden–Julian oscillation on storm-track activity, surface air temperature, and precipitation over North America. *Journal of Climate*, *31*(15), 6113–6134. https://doi.org/10.1175/JCLI-D-17-0534.1

Zhou, W., Yang, D., Xie, S. P., & Ma, J. (2020). Amplified Madden–Julian oscillation impacts in the Pacific–North America region. *Nature Climate Change*, *10*(7), 654–660. https://doi.org/10.1038/s41558-020-0814-0

Zhu, Y., & Newell, R. E. (1998). A proposed algorithm for moisture fluxes from atmospheric rivers. *Monthly Weather Review*, *126*(3), 725–735. https://doi.org/10.1175/1520-0493(1998)126<0725:APAFMF>2.0.CO;2